Difluoro Dipyridomethene Boron Complexes: Synthesis, Characterization, and Ab Initio Calculations

Carlotta Figliola, Alexandra Sutter, Thomas Papineau, Camille Chériaux, Pascal Retailleau, Denis Jacquemin, Gilles Ulrich

Difluoro dipyridomethene boron complexes: synthesis, characterization, and *ab-initio* calculations

Carlotta Figliola,*[a] Alexandra Sutter,[a] Thomas V. Papineau,[b] Camille Chériaux,[a] Pascal Retailleau,[c] Denis Jacquemin,*[b,d] Gilles Ulrich*[a]

[a] Institut de Chimie pour l'Energie, l'Environnement et la Santé (ICPEES), UMR CNRS 7515, Université de Strasbourg, 25 rue Becquerel, 67087 Strasbourg Cedex 02, France

[b] Nantes Université, CNRS, CEISAM UMR 6230, F-44000 Nantes, France

[c] Service de Cristallographie Structurale, ICSN-CNRS Université Paris-Saclay, 1 Avenue de la Terrasse, Bât.27, 91198 Gif-sur-Yvette Cedex, France

[d] Institut Universitaire de France (IUF), F-75005 Paris, France

corresponding authors e-mail: figliola@unistra.fr, denis.jacquemin@univ-nantes.fr, gulrich@unistra.fr

Abstract

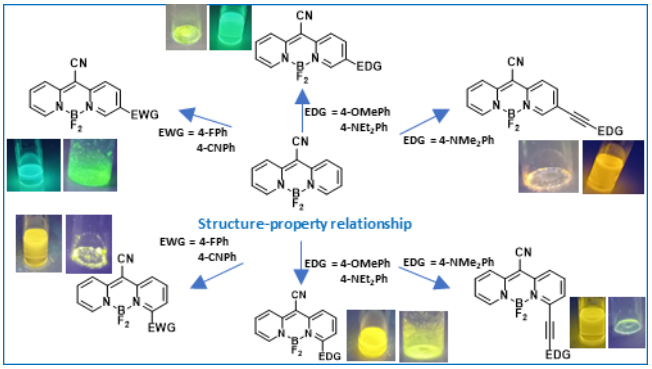

Molecular engineering studies on the *meso*-cyano difluoro dipyridomethene boron complexes are presented and two series (**a** and **b**) of novel fluorophores are extensively studied. Halogenated derivatives were reacted under Suzuki-Miyaura or Sonogashira cross coupling reactions to introduce electron-donating or electron-withdrawing functional groups on positions 1 and 2 of the aromatic ligand. All derivatives were obtained in 14-90% yields and studied in detail by structural, photophysical and computational analyses. Both series display excellent emissive properties in solution with blue to orange fluorescence emission upon blue light absorption and promising features as solid emitters. All the spectroscopic measurements are supported and confirmed by first-principles theoretical calculations combining TD-DFT and CC2. Series **b**, featuring an aryl substituent onto position 1 of the aromatic core, showed significantly large Stokes shifts values.

Introduction

In recent years, polycyclic aromatic systems have been at the center of the research developing advanced fluorescent materials, optoelectronic devices, biological probes, and theranostic systems. [1] Functionalization with main group elements, such as boron and nitrogen, not only increases the structure diversity but also confers novel physical and chemical properties. [2, 3] The presence of nitrogen-boron bonds into polycyclic aromatic structures, *e.g.* naphthalene, [4, 5] anthracene, [6] phenanthrene, [7] and perylene backbones, [7] led to improvements of their physical and spectroscopic properties compared to the corresponding all-carbon parent structure. [8] Four-coordinated nitrogen-chelated boron complexes is an effective strategy to obtain photoluminescent compounds. [9] Indeed

boron complexation increases molecular rigidity and planarity of the aromatic core leading to highly fluorescent dyes. [2, 10, 11, 12, 13] Among the four-coordinated boron-containing fluorescent dyes, [14, 15, 16] 4,4-difluoro-4-bora-3a,4a-diaza-s-indacenes (BODIPYs) are by far the most developed. [17, 18, 19, 20, 21, 22, 23, 24] Their synthetic versatility, high extinction coefficient (ε) and often large fluorescence quantum yields (ϕ_F), good chemical robustness and stability found a wide range of applications in various areas, *e.g.* biological sensors, imaging agents, lasers, electroluminescent devices, as well as solar cells. [17, 18, 19, 20, 21, 22, 23, 24] However, their application as thin films in organic light emitting diodes, in aqueous media for sensing and imaging is limited because of the highly planar structure and extended π-conjugation of BODIPYs inducing π-π stacking and aggregation, quenching the emissive properties. [14, 16] Furthermore, they exhibit small Stokes shift values, leading to self-absorption processes and subsequent detrimental photobleaching. [25] To overcome these limitations, the development of BODIPY analogues remains an active research area. [9, 26]

Compared to BODIPYs and despite the presence of the pyridine as chelating ligand, which enhances the fluorescent emission properties [27, 28, 29, 30, 31, 32, 33] it is striking to see how little the four-coordinated difluoro dipyridomethene boron complexes, also known as BF_2-DIPYRs, has been investigated. Beside the initial synthetic reports, [34, 35] the first description of the physical and spectroscopic properties as well as the synthetic diversification of the structure was reported only recently. [9, 36]

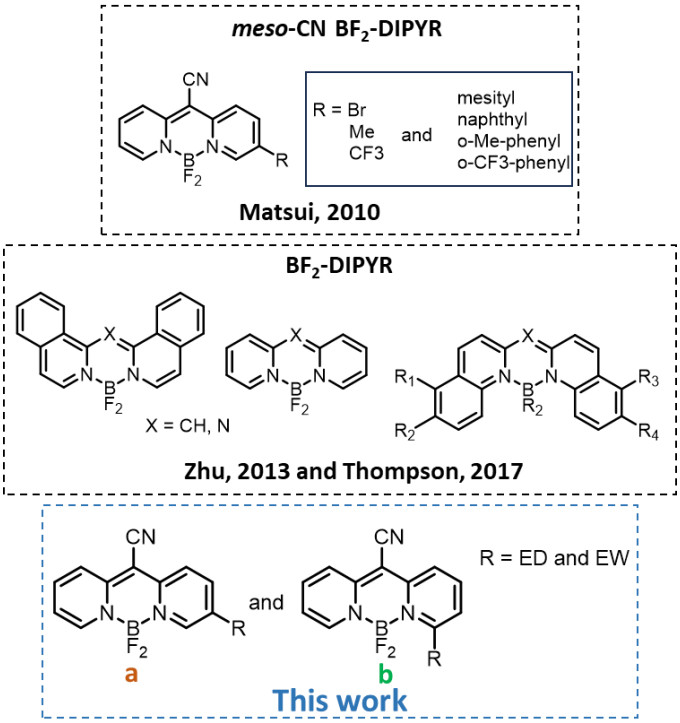

Figure 1. Reported BF_2-DIPYR dyes and targeted compounds in the present work.

Meso-cyano (*meso*-CN) BF_2-DIPYR complex and the corresponding 2-substituted derivatives show moderate fluorescence emission both in solution and in the solid state (Figure 1).[36] Later, this scaffold found applications as emitters in solar cells and as chemosensors for hydrazines. [37, 38] A detailed study on BF_2-DIPYR (X = CH, Figure 1) as well as the corresponding quinoline- and isoquinoline-based complexes was reported in 2017 only. [39] Except for the unsubstituted parent compound, the π-extended derivatives display similar spectroscopic properties to BODIPY dyes with relatively high molar absorption, good photostability, and efficient green fluorescence emission in solution. [39] Dimers of the latter show valuable symmetry-breaking charge-transfer features for further applications in optoelectronic technologies. [40] The corresponding aza-BF_2-DIPYRs (X = N, Figure 1) have been also synthetized. [41, 42, 43, 44] Compared to the aza-BODIPYs absorbing and emitting light in the red/near

infrared (NIR) region, [45, 24, 22] replacing the *meso* carbon with a nitrogen in the BF_2-DIPYR scaffold induces a hypsochromic shift of both absorption and emission wavelengths, [41, 42, 43, 44] which has been exploited in white organic light emitting diodes (WOLEDs) applications. [41, 44]

Herein, we report our molecular engineering study on the *meso*-CN BF_2-DIPYR complexes *via* the introduction of electron-donating and withdrawing functional groups on positions 1 and 2 of the aromatic ligand core (Figure 1) to extend the structure-property relationship on the *meso*-CN BF_2-DIPYR, which had, until now, only included examples with bulky substituents in position 2.[36] Two series of mono-substituted *meso*-CN complexes (**a** and **b** in Figure 1) were synthetized in good to high yields and characterized thoroughly, including by X-ray diffraction analysis. Spectroscopic measurements, fruitfully rationalized by *ab initio* calculations, are reported showing excellent fluorescence properties in solution with colors from blue to orange upon blue light absorption and promising features as solid emitters. Opposite to similar compounds, the **b** series also displays remarkably large Stokes shifts values.

Results and discussion

Synthesis

The synthetic strategy for the preparation of boron complexes **3-7a,b** is shown in Scheme 1 and Scheme 2. Following an earlier report, [36] brominated *meso*-CN-dipyridomethene **1a,b**[46] reacted with boron trifluoride in the presence of triethylamine yielding the corresponding BF_2-complexes **2a,b** (86% and 84%, respectively). Subsequent Suzuki-Miyaura cross coupling reaction afforded the final fluorophores **3-6a,b** in moderate to high yields (Scheme 1).

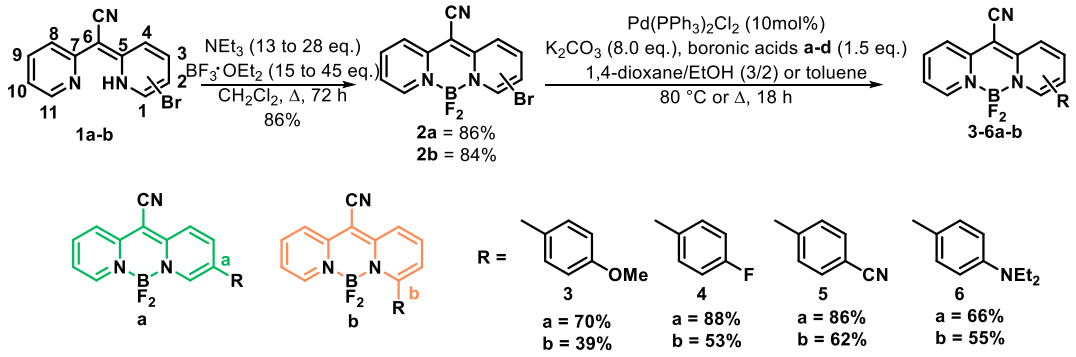

*Scheme 1. Synthesis of the aryl-substituted meso-cyano BF_2-complexes **3-6a,b** via Suzuki-Miyaura cross-coupling reaction. The numbering of **1a-b** and the corresponding complexes (two examples in Figure 2) follows the previous work in ref. 39 for better comparison of similar compounds.*

To increase the distance between the BF_2-DIPYR core and the aryl substituent, complexes **7a-b** featuring an aniline-substituted triple bond were targeted *via* a Pd-catalyzed Sonogashira cross coupling. While boron complex **7a** was obtained from **2a** *via* Sonogashira cross coupling reaction (Scheme 2), the corresponding complex **7b** was obtained through BF_2-complexation of the ligand **8**, already functionalized by ethynyl-extended aniline derivative under Sonogashira cross coupling reaction conditions (Scheme 2). Indeed, compound **2b** showed to be prone to degradation and dehalogenation under the reaction conditions used for the synthesis of **7a**. It is probably because of the steric hindrance of position 1 on **2b** compared to position 2 on **2a** slowing the oxidative insertion of the catalyst and favoring other side reactions. This might also explain the low yields of **7b** and the other **b** complexes (Scheme 1).

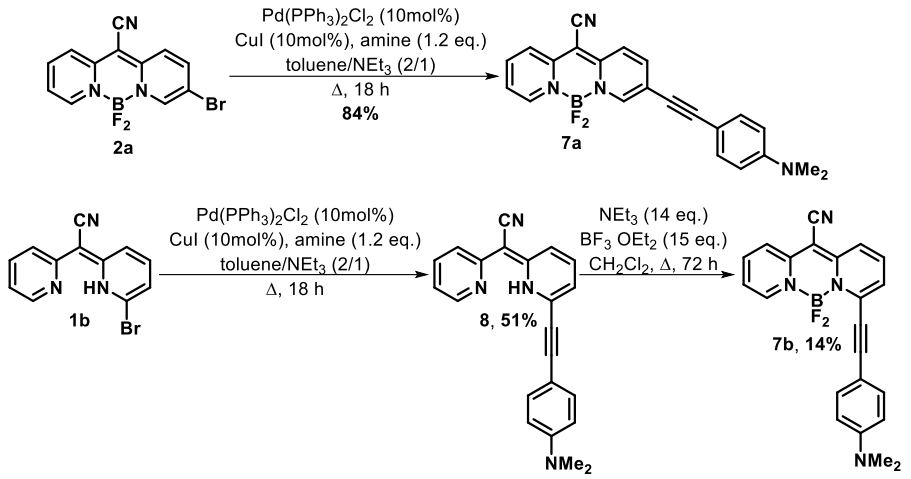

*Scheme 2. Synthesis of the aryl-substituted 2-cyano BF_2-complexes **7a,b** via Sonogashira cross-coupling reaction.*

The final structures and all the intermediates were characterized by NMR spectroscopy (^{1}H, ^{13}C, ^{11}B and ^{19}F) and HRMS, see Supporting Information (SI).

Interestingly, as previously observed by Thompson *et al.* for similar DIPYR derivatives, [39] ^{1}H NMR of the BF_2-complexes **3a-7a** feature the pyridyl α protons, H1 and H11, as broad singlets instead of the expected singlet and doublet, respectively, because of the short intramolecular H···F distances (**3a** is shown in Figure 2 as example). In the DFT calculations the H11 and H1 and the closest fluorine are indeed quite close from one another (2.32 Å). However, this does not significantly affect the resonance of the corresponding carbons, which are shown as broad singlets.

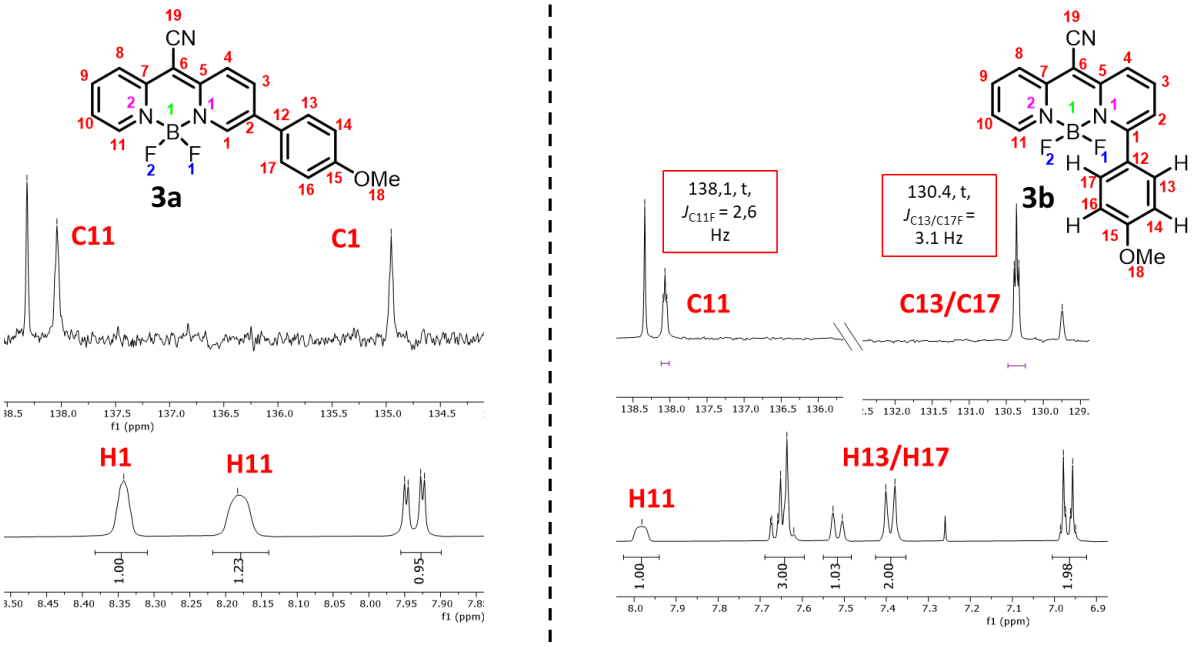

*Figure 2. ^{1}H and ^{13}C NMR spectra analysis of dyes **3a** (left) and **3b** (right).*

Concerning the BF_2-complexes **3b-7b**, ^{1}H and ^{13}C NMR suggest a proximity of both the aryl *ortho* protons, H13 and H17, and the *ortho* pyridyl proton, H11, with the fluorine atoms bound to the boron center (**3b** is shown in Figure 2 as example). Notably, the CH show a broadening of the expected doublets in the ^{1}H NMR spectrum and the corresponding carbons are clearly resolved into a triplet (δ = 130.4 ppm, $J_{C13/C17F}$ = 3.1 Hz and δ = 138.1 ppm, J_{C11F} = 2.6 Hz for **3b**) because of the through-space coupling to the ^{19}F atoms. DFT optimizations lead to a rather short H17···F1 distance of 2.34 Å in **3b**,

smaller than the sum of van der Waals radii, consistent with a non-trifling interaction (see also below for XRD/DFT comparisons of other compounds).

Structural properties

Single crystals of **5a,b** were obtained by slow evaporation of deuterated chloroform and the corresponding molecular structures were obtained by X-ray diffraction as shown in Figure 3 and Figure S4. As general analysis of the structure, the carbon-carbon bond lengths of the DIPYR aromatic core in **5a,b** are consistent with those of similar boron complexes and the anthracene (Figure S4, a). [36, 39, 47] As previously observed, C−N bond lengths, notably C1−N1, C5−N1, C7−N2 and C11−N2 in **5a,b** (Figure S4, a), are longer (averaged values ≥1.36 Å, closer to 1.38 Å on the side of the substitution) than the values found in the pyridine (1.337 Å) and closer to those in anthracene, because the boron chelation reduces the electron density on the nitrogen and thus the polarization of the corresponding C−N bond. The N−B (averaged value 1.56Å from 1.550(4) to 1.575(2) Å) and B−F (1.375 from 1.368(4) to 1.393(4)Å) distances indicate a significant polarization of the corresponding bonds and they are all in the typical range found in molecular analogues (including BODIPY derivatives). Similarly, the central ring adopts an intermediate conformation between screw-boat and boat, [48] with the -BF_2 group lying above the aromatic plane, as it is also observed as in previous examples (Figure S4, b). DFT reproduces this very same conformation in the simulations made in solution, so it does not result from solid-state packing.

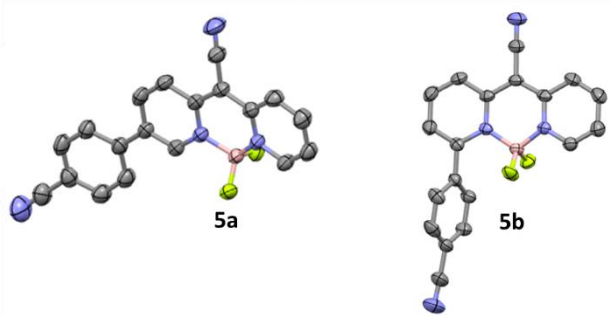

*Figure 3. Molecular structure of **5a,b**; displacement ellipsoids are drawn at the 50% probability level. For **5a** only one conformer out of three present in the asymmetric unit as well as a disordered deuterated chloroform molecule, is shown for clarity.*

Regarding the arrangement of the aryl groups towards the DIPYR core, the torsion angles were obtained in the range of 3.4-7.7° (**5a**) and 69.5° (**5b**), suggesting that the substituent in position 2 is almost co-planar with the central aromatic scaffold, while that in position 1 is almost perpendicularly twisted. Interestingly, DFT optimizations carried out in solution deliver the following torsional angles: 37.8° (**5a**) and 68.1° (**5b**). This indicates that while the torsions in **5b** are intrinsic to the system, the very small distortion in the X-ray structure of **5a** probably comes in part from packing effects, as a ca. 30° discrepancy between theory and measurements is unlikely to stem from the DFT inaccuracies only (note that we used a functional that is known to be adequate for dispersion effects). Crystal packing of **5a** and **5b** were obtained and used as references for the two series of dyes (Figure 4, Figure 5 and Figure S9).

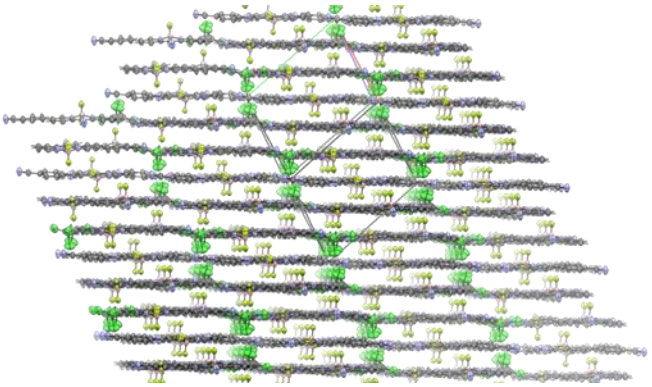

*Figure 4. Partial view of the crystal packing of **5a** in layers (a) parallel to the (111) plane.*

5a crystallized in a centrosymmetric triclinic unit cell composed of six molecules (three independently refined conformers A, B and C) and some voids partially occupied by deuterated solvent $CDCl_3$ molecules. Quasi-planar molecules **5a** (rsmds for the 23 non-H atoms except BF_2 are 0.1435, 0.1688 and 0.0751Å and dihedral angles between DIPYR and the Phe-CN are 6.6, 7.7 and 3.4° for A, B and C conformers, respectively) lie in successive layers parallel to (111) plane with a regular interplanar distance of ca 3.3 Å, despite an alternative stacking pattern along the [101] direction (A∀/BↃ/Ɓ C layers with solvent molecules dispersed between the A∀/BↃ interlayer). Per layer, the elongated molecules **5a** with the benzonitrile substituent in C2 are oriented in an antiparallel way along the [-110] direction. In fine, the molecules infinitely stacked with their different aromatic groups overlapping at centroid-to-centroid distances in the range of 3.65-3.85Å (Figure S9, c). **5b**, which are substituted in C1, crystallized in a centrosymmetric monoclinic unit cell with one molecule in the asymmetric unit. **5b** packed in a herringbone fashion but without optimal overlap between the aromatic rings (the centroid-to-centroid distances exceed 4.7Å in the crystal packing, Figure 5).

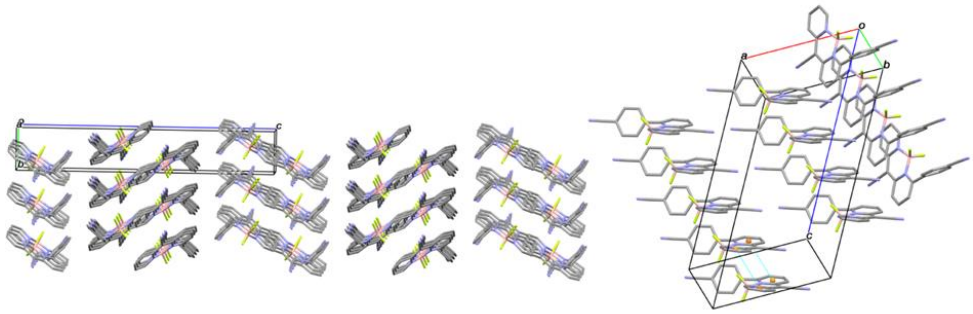

*Figure 5. Partial views of the crystal packing of **5b** down the **a** axis (left). Zoom on the molecular DIPYR stacking showing no close π-π interactions (orange dots are the hetero, 6-members centroids dotted lines in cyan underscore distances > 4.7Å).*

Photophysical properties

The photophysical properties of boron complexes **3-7a,b** were characterized by UV/Vis absorption and emission spectroscopy in both solution and the solid state (Table 1 and Table S1 for series **a**, Table 2 and Table S2 for series **b**). UV/Vis and emission spectra are shown in Figure 6 (**3a** and **5a**), Figure 7 (**6a/6aH$^+$**), Figure 8 (**3b** and **5b**) and Figure 9 (**6b**) as well as in Figure S1 (**4a** and **7a/7aH$^+$**) and Figure S2 (**4b**, **6bH$^+$**, **7a/7aH$^+$**). Emission spectra of **3-7a,b** in the solid state are shown in Figure S3.

*Table 1. Photophysical data of **2a** (hexane) and **3-7a** (p-xylene) in solution and in solid state at room temperature.*

	Solution									Solid	
	λ_{abs} (nm)	ε (x 10^4 M^{-1}·cm^{-1})	F_{max} (nm)	ΔE (eV)	ΔSS (cm^{-1})	ϕ_F (%)[a]	τ (ns)	k_r (s^{-1})	k_{nr} (s^{-1})	F_{max} (nm)	ϕ_F (%)
2a[36]	451	2.4	473		n.d.	3	n.d.	n.d.	n.d.	513	0.02

3a	461	3.4	477	2.64	768	38	2.4	1.58×10^8	2.58×10^8	514	3.0 (±0.13)
4a	457	3.9	472	2.67	647	46	2.6	1.80×10^7	2.12×10^8	520	1.0 (±0.03)
5a	461	4.5	475	2.64	639	43	2.0	2.15×10^8	2.85×10^8	518	<1 (±0.02)
6a	472	3.1	500	2.55	1186	44	2.4	1.83×10^8	2.33×10^8	542	2.0 (±0.02)
6aH$^+$[b]	460	3.0	474	2.65	642	38	2.3	3.48×10^7	4.00×10^8	n.d.	n.d.
7a	471	4.6	491	2.57	865	51	2.1	2.43×10^8	2.33×10^8	565	7.0 (±0.03)
7aH$^+$[b]	466	4.3	490	2.59	1051	47	2.1	2.24×10^7	2.52×10^8	n.d.	n.d.

[a] ϕ_F were calculated by using Rhodamine 6G as a reference (λ_{exc} = 488 nm, ϕ_F = 0.88 in EtOH); [b] protonation was performed by bubbling HCl vapors in the solution containing **6a** and **7a**.

The *meso*-CN BF_2-DIPYR complexes **3-7a** display a main absorption band corresponding to the S_0-S_1 transition with extinction coefficients of similar intensity to other reported DIPYR derivatives ($\varepsilon = 10^4$ $M^{-1} \cdot cm^{-1}$, Table 1). Increasing the solvent polarity induces a small hypsochromic shift together with an intensity increase of the less defined 0-1 vibronic transitions as compared to the 0-0 one, independently of the electronic nature of the phenyl substituent in position 4 (Figure 6 and Figure S1). Theoretical calculations on both **3a** and **3b** (see below) indicate a small decrease of the magnitude of the dipole moment in going from the ground to the excited state, which is consistent with negative solvatochromism. As expected, this vibronic band becomes less defined when going from nonpolar solvents (toluene and/or *p*-xylene) to the most polar one (DMSO). Adding electron-rich substituents on the phenyl group, notably NEt_2 and NMe_2, induces a significant bathochromic shift of the main absorption band compared to electron-deficient groups, *i.e.* -F and -CN. Furthermore, the broadening of the band and the loss of differentiation between the two vibronic transitions suggest that a sizeable intramolecular charge-transfer (ICT) character is present and follows the NEt_2Ph > NMe_2Ph-≡ > OMePh > FPh > CNPh order (Figure 7 and Figure S1). To study how the change of the induction effect influences the spectroscopic behavior of complexes **6-7a**, protonation of the amino group with HCl vapors is performed. Even if the ε of the corresponding **6aH$^+$** and **7aH$^+$** is not significantly affected, it induces a narrowing as well as a hypsochromic shift of the main absorption band as compared to the non-protonated form, clearly in the line with a strong reduction of the ICT, getting back to a S_1-S_0 emission observed in nonpolar solvents (Figure 7 and Figure S1). Concerning the fluorescence emission, *meso*-CN BF_2-DIPYR complexes **3-5a** are luminescent in solution with excellent fluorescence quantum yields (ϕ_F) of 40-50% and large Stokes shifts (ΔSS, Table 1 and Table S1) increasing with the solvent dipole moment reaching a maximum in DMSO of 1193 cm^{-1} (**3a**), 1214 cm^{-1} (**4a**) and 1092 cm^{-1} (**5a**). Furthermore, the emission shows a small enhancement of the ICT band, which leads to a slight shift of the S_1-S_0 peak with the increase of the solvent polarity, and it appears as a well-resolved symmetric mirror-image of its absorption counterpart (Figure 6 and Figure S1).

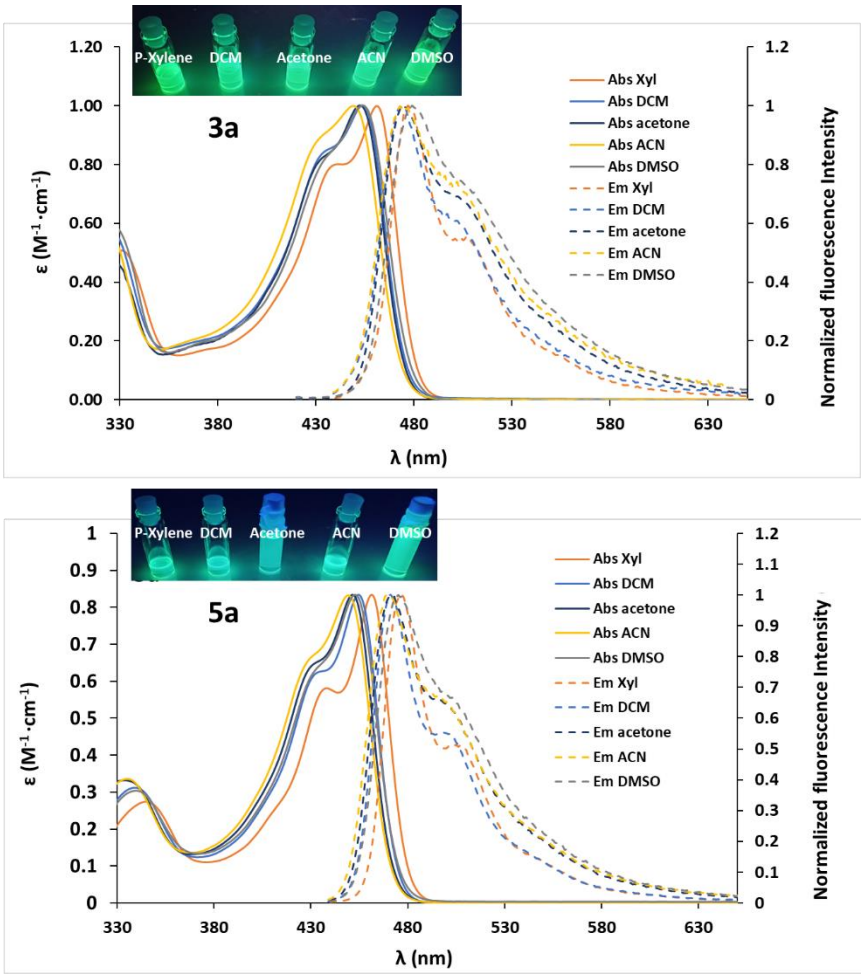

*Figure 6. Absorption (plain line) and emission (dotted line) spectra of dyes **3a** and **5a** in multiple solvents.*

In the case of **6a**, the emission band is well-structured in nonpolar solvents, while increasing the solvent polarity gives a significant bathochromic shift, a poorer vibronic resolution (Figure 7) as well as an enhanced ΔSS reaching a maximum of 4277 cm^{-1} in DMSO (Table S1). However, the ϕ_F of **6a** drops dramatically when going from nonpolar to polar solvents, consistent with a solvatochromic system switching from a localized excited state to a low-lying ICT one.

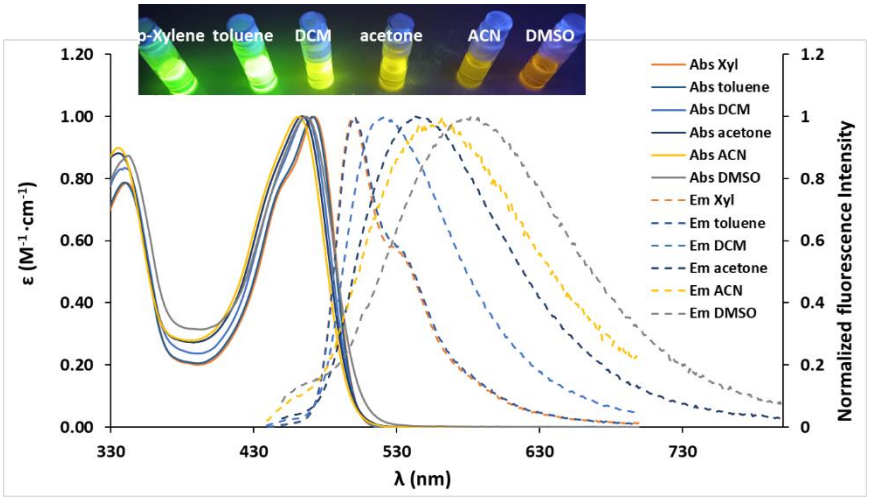

*Figure 7. Absorption (plain line) and emission (dotted line) spectra of dye **6a** in multiple solvents.*

The emissive properties of **7a** are similar to those of **6a** (Table 1, Table S1, and Figure S1). However, the fluorescence emission band of **7a** becomes more and more difficult to interpret in ACN and DMSO (Figure S1), suggesting emission from two different forms, *e.g.* the neutral and the protonated structures. Nevertheless, vapors of NEt_3 were added to neutralize the solution and no changes were observed. Upon protonation of **7a** a hypsochromic shift of the maximum peak is observed with no impact of the polarity of the solvents and excellent ϕ_F (40-50%, Table S1), resembling the behavior of **6a**.

The fluorescent lifetimes of complexes **3-7a** are all in the nanosecond range with significant non-radiative rate constants, both values are expected for organic fluorescent compounds.

*Table 2. Photophysical data of **3-4b** (p-xylene), **2b, 5-6b/6bH⁺** (toluene) and **7b** (dichloromethane) in solution and in solid state at room temperature.*

	Solution									Solid	
	λ_{abs} (nm)	ε (x 10^4 M^{-1}·cm^{-1})	F_{max} (nm)	ΔE (eV)	ΔSS (cm^{-1})	ϕ_F (%)[a]	τ (ns)	k_r (s^{-1})	k_{nr} (s^{-1})	F_{max} (nm)	ϕ_F (%)
2b	460	2.6	480	2.65	906	1	n.d.	n.d.	n.d.	n.d.	n.d.
3b	454	2.5	553	2.68	3895	15	2.1	7.14 x 10^7	4.05 x 10^8	528	3.0 (±0.03)
4b	454	2.8	551	2.65	4008	6	1.1	5.45 x 10^7	8.55 x 10^8	505	2.0 (±0.01)
5b	455	2.3	588	2.55	4971	≈1	n.d	n.d	n.d	542	6.0 (±0.02)
6b	456	2.6	564	2.55	4337	35	3.4	1.03 x 10^8	1.91 x 10^8	522	8.0 (±0.07)
6bH⁺[b]	456	2.2	n.d	n.d	n.d	n.d	n.d	n.d	n.d	n.d.	n.d.
7b	471	1.7	528	2.44	2292	44	5.0	8.74 x 10^7	1.11 x 10^8	569	2.0 (±0.01)
7bH⁺[b]	460	1.1	581	2.42	4527	4	1.0	4.21 x 10^7	1.01 x 10^9	n.d.	n.d.

[a] ϕ_F were calculated by using Rhodamine 6G as a reference (λ_{exc} = 488 nm, ϕ_F = 0.88 in EtOH); [b] protonation was performed by bubbling HCl vapors in the solution containing **6b** and **7b**.

As for the *meso*-CN BF_2-DIPYR complexes of series **a**, the corresponding series **b** also absorbs light in the UV/Vis blue region with ε of 10^4 M^{-1}·cm^{-1} (Table 2 and Table S2). The main absorption band corresponding to the S_0-S_1 transition appears structured in *p*-xylene, while it becomes significantly broader and less defined in more polar solvents with a small hypsochromic shift of the maximum peak (Figure 8 and Figure S2). Furthermore, in contrast to the **3-7a**, the electronic nature of the substituents on the phenyl group in **3-6b** affects neither the absorption wavelength nor the intensity (Table 2 and Table 2S). However, the combination of a π-extended conjugation and the electron-donating nature of the tertiary aniline in **7b** induces a significant bathochromic shift of the absorption maximum peak as for the corresponding **7a** (Figure S1). Due to the poor solubility of **7b** in most of the tested solvents except dichloromethane, it was not possible to analyze the effect of solvent polarity on the absorption profile.

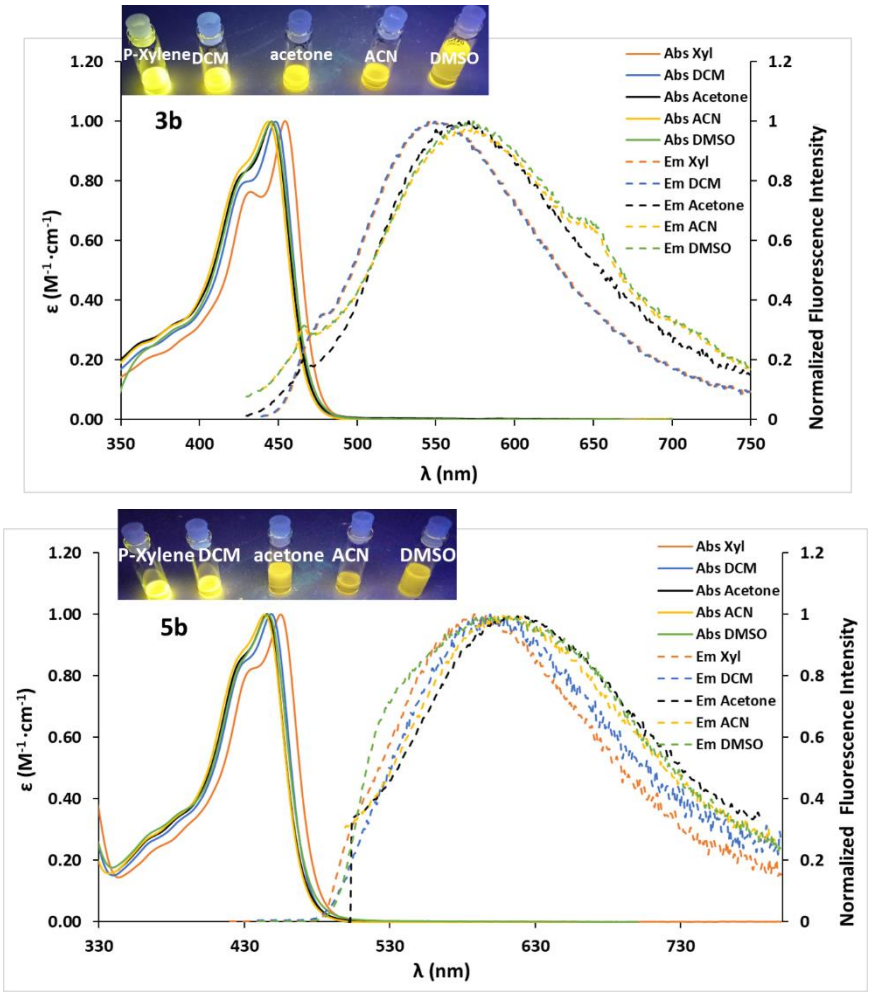

*Figure 8. Absorption (plain line) and emission (dotted line) spectra of dyes **3b** and **5b** in multiple solvents.*

BF_2-DIPYR derivatives **3-6b** display a very broad and unstructured fluorescence emission band whose maximum peak is slightly bathochromically shifted with the increase of the solvent dipole moment (Figure 8, Figure 9 and Figure S2). Large ΔSS, in the 3000-6000 cm^{-1} range, with a maximum in DMSO are observed for **3-6b** (Table 2). Dyes **3-5b** are weakly luminescent with ϕ_F values dropping in polar solvents (Table S2). Theoretical calculations on both **3b** and **5b** (see below) indicate a remarkable change in the geometry of the complexes upon excitation, especially in **5b**. This induces a significant ICT character with a decrease in the ϕ_F values going from nonpolar to polar solvents. It also explains why the fluorescence emission is no longer the mirror-image of the absorption counterpart and, consequently, the large Stokes shifts. Notable exceptions are complexes **6-7b** that stand out as the most fluorescent dyes in the series with ϕ_F values of 35% for **6b** and 44% for **7b** decreasing slightly in polar solvents (Table 2 and Table S2). Upon protonation of the tertiary anilines, the main absorption band remains unvaried, while the fluorescence emission is quenched. Concerning the **7bH$^+$**, the main absorption band becomes broader, more unstructured and hypsochromically shifted compared to **7b**. In contrast to **6bH$^+$**, it displays still a residual fluorescence emission with ϕ_F of about 4%.

As for the **a** series, the corresponding **3-7b** also show short fluorescent lifetimes because of the strong non-radiative component of the excited complex deactivation.

The low values of ϕ_F of derivatives **2a-b** (Table 1 and Table 2) are consistent with substitution of the fluorescent aromatic BF_2-DIPYR core with halogen, which enhances the intersystem crossing (ISC) and the excited triplet state (T_1) generation. The steady-state spectrum at low temperature showing the emission of both the singlet and the triplet emission of the novel compound **2b** has been recorded in

methyl tetrahydrofuran at 77 K and it shows as a peak at 540 with a vibronic shoulder at 580 nm (Figure S 4). As expected, the fluorescence emission at 77 K is more structured with well-defined vibrational transitions compared to that at room temperature (Figure S 5).

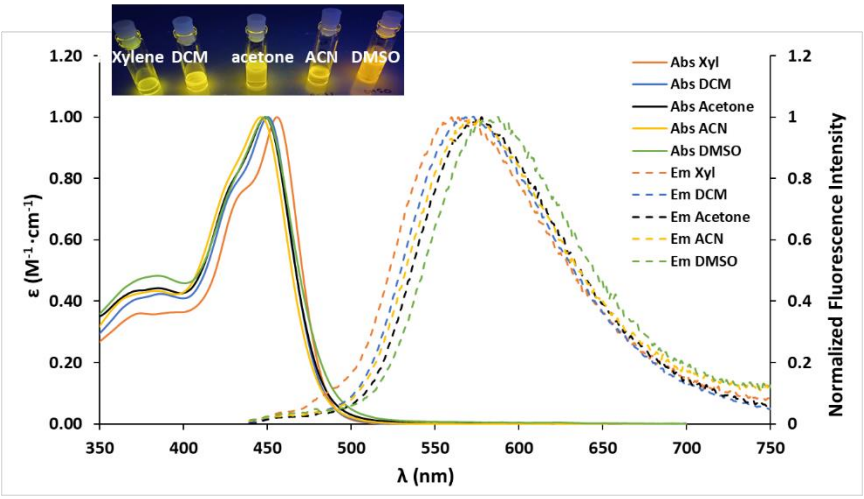

*Figure 9. Absorption (plain line) and emission (dotted line) spectra of dye **6b**.*

In contrast to other boron complexes, notably BODIPY[14, 15] and previous BF_2-DIPYR derivatives shown in Figure 1,[40] all the synthesized complexes **3-7a,b** exhibit fluorescence in the solid state with maxima in the 500-560 nm range. Compared to the previously reported *meso*-CN BF_2-DIPYRs, [36] dyes **3-7a,b** display moderate emissive properties independently of the conformation (planar and more twisted for the **a** and **b** series, respectively) or the electronic nature of the phenyl substituent. As shown by the observed crystal packing, the π-π network observed for the series **a** could cause fluorescence quenching in the solid state and low ϕ_F. In contrast, the crystal packing of series **b** with no π-stacking or other intermolecular interactions display more efficient emissive properties in the solid state (ϕ_F = 6% in Table 2).

Theoretical calculations

First-principles calculations were used to obtain additional insights into the excited-state properties of the synthesized compounds, using a theoretical approach described in detail in the SI. The main spectral data are listed in Table 3. The 0-0 energies do offer a ground for meaningful theory-experiment comparisons and the mean absolute deviation between experiment and theory is very small (0.06 eV), which clearly indicates that the level of theory selected is suited for our purposes. Furthermore, the main trends, measured for the 0-0 energies, the absorption, and fluorescence wavelengths, are reproduced by calculations. However, the vertical absorption and emission wavelengths listed in Table 3 can only be qualitatively compared to the experimental maximal absorption and emission.

*Table 3. Computed vertical absorption and emission wavelengths in nm, as well as 0-0 energies in eV for all compounds in p-xylene but for **2a** (hexane) and **2b** (toluene)*

Compound	$\lambda_{vert\text{-}abs}$ **(nm)**	$\lambda_{vert\text{-}fluo}$ **(nm)**	$\Delta E^{0\text{-}0}$ **(eV)**
2a	409.4	476.3	2.657
2b	411.4	513.1	2.646
3a	416.3	454.8	2.664
3b	411.2	482.7	2.659
4a	413.8	449.4	2.690
4b	409.9	498.4	2.646
5a	417.9	454.5	2.671
5b	411.5	551.8	2.509
6a	429.3	484.5	2.532
6aH⁺	420.1	461.8	2.621
6b	420.3	486.8	2.597

6bH$^+$	411.8	592.9	2.474
7a	434.4	477.4	2.541
7aH$^+$	428.5	468.2	2.573
7b	440.7	508.0	2.442
7bH$^+$	441.9	598.0	2.184

One of the most striking experimental findings is that in nonpolar solvents, the **a** and **b** series give rather similar absorption spectra, yet very different fluorescence profile: the fluorescence of the **a** derivatives is mostly the mirror image of the absorption, whereas that of the **b** compounds has more redshifted and lower vibrational resolution, typical of an ICT fluorescence. The theoretical simulations do reproduce this effect. Illustratively, let us compare **3a** and **3b** as well as **5a** and **5b**, the former being substituted by donor group (anisole), the latter by an accepting group (benzonitrile). The absorption of **3a** is redshifted by 6 (5) nm as compared to **3b** experimentally (theoretically), and similar values are obtained when comparing **5a** and **5b** (6 (6) nm). In both cases, the ordering of the compounds can be easily intuited: in the **a** series the side groups are almost coplanar whereas steric effects induce a less planar conformation in the **b** series. For instance, the (ground-state) dihedral angle between the core of the dye and the side phenyl ring is 38° in **3a** but 64° in **3b**. Interestingly, the ordering is reversed for fluorescence, **3b**'s emission spectra being bathochromically shifted by 76 (28) nm experimentally (theoretically). Again, the values for **5a/b** show the same trends 113 (98) nm, but they cannot be explained by simple geometric considerations. We recall that due to the lack of vibronic couplings (see also below), such theory/experiment comparison remains qualitative, yet the key trend is restored. To understand why such unexpected inversion occurs, we provide in Figure 10, electron density difference plots (EDDs) for both absorption and emission for all these four compounds. For both **3a** and **5a**, these plots reveal that the density changes are mostly located on the dipyrrin core, with a significant contribution of the central cyano moiety but rather small involvement of the side groups, consistent with the fact that **3a** and **5a** have similar absorption spectra. Furthermore, the EDDs for both absorption and emission of these two compounds, are almost perfectly inverted, consistent with the rather small Stokes shift and the mirror-image absorption and emission spectra (Figure 10). In **3b** and **5b**, the absorption EDDs are essentially equivalent to their **3a** and **5a** counterparts, the side groups playing almost no major role, again fitting experimental trends (Figure 10). However, the fluorescence EDDs are no longer the symmetric of their absorption counterparts, but show rather significant ICT character, especially in **5b** (Figure 10). This is likely due to a significant change of geometry allowing some excited-state pseudo- symmetry breaking. Indeed, in **3b**, the above-mentioned dihedral angle goes from 64° in the ground state to 44° in the excited state. The analysis of the EDDs provides a distance between the electron and hole barycenter of 0.71 Å (1.06 Å) for absorption but 1.71 Å (2.63 Å) in **3b** (**5b**) for emission, clearly underlying the increase of ICT character after excited-state relaxation.

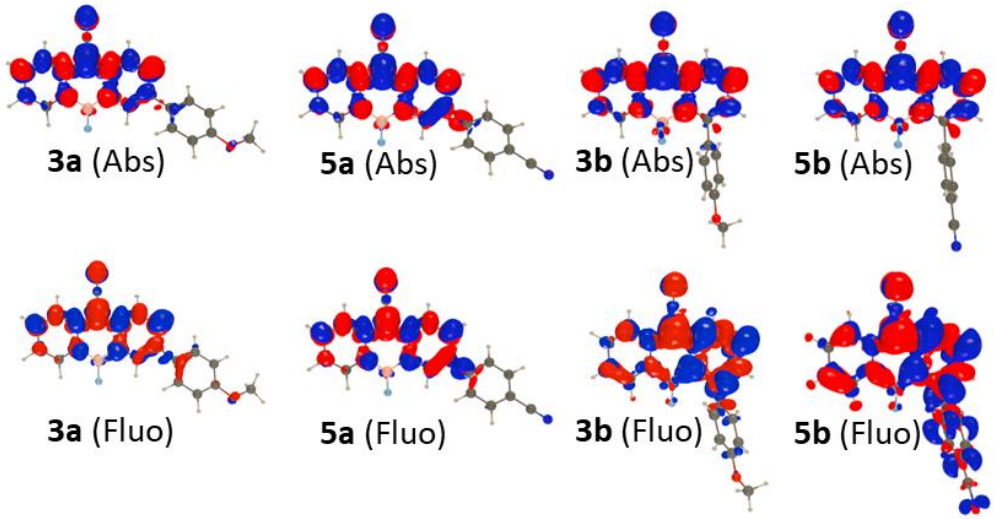

*Figure 10. Electron Density Difference (EDD) representation for both absorption and emission of **3a** and **3b**. A contour threshold of 0.001 au is used. The blue and red lobes represent region of decrease and increase of electron density upon transition, respectively.*

To go further, we have modelled the vibronic couplings in **3a** and **3b** (see the SI for details). The resulting vibrationally-resolved spectra are displayed in Figure 11. Some vibrational resolution emerges for both compounds in absorption, with the longest wavelength peak being significantly dominant in **3b**, but not in **3a**. The experimental absorption bands of the two compounds are more alike and in between the one simulated by theory. More interesting are the differences in the emission profile. **3a** features a vibronic progression and a relatively thin spectrum, whereas **3b** shows a broader less resolved emission band, consistent with the experimental findings.

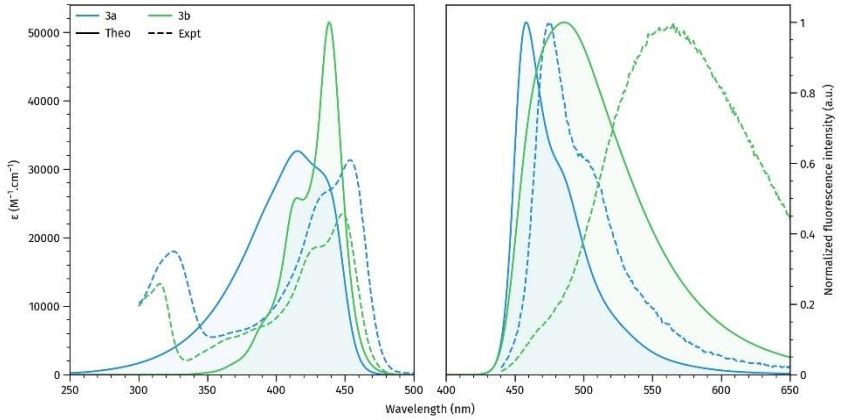

*Figure 11. Simulated vibrationally-resolved spectra (full line) and experimental spectra (dotted line) of **3a** (blue) and **3b** (green), considering both absorption (left) and emission (right). For an easier comparison of the band shapes, the figure where the simulated spectra are shifted to match the experimental ones is in the SI as Figure S12.*

Regarding the amino-substituted dyes **6a/b** and **7a/b**, the EDD plots are displayed in Figure 12 for the **a** series and Figure 13 for the **b** series. The donor character of the amino group is present, but it remains limited in both **6a** and **7a**. These small contributions are consistent with the small absorption redshifts as compared to the other members of the **a** series (ca + 10 nm). As expected, protonation of the amino group makes the side moiety a passive element in the excited state, and the redshift vanishes. Concerning the amino derivatives in the **b** series, while the absorption of **6b** and **7b** are not much affected by protonation (as in the **a** series), the fluorescence emission of **6b** is quenched and that of **7b** is strongly redshifted upon protonation. Both results are reproduced by theory (Table 3). As it can be observed from the EDDs of **7b** in Figure 13, the emission EDD is almost the mirror-image of its

absorption counterpart, consistent with the experimental spectra of Figure S2. In contrast to the **a** series, protonation does not simply quench the donor character of the amino group, it induces a significant ICT from the core of the dye towards the ammonium moiety (as for absorption). This ICT is consistent with the strong decrease of the emission yield noticed in the **7b** after protonation.

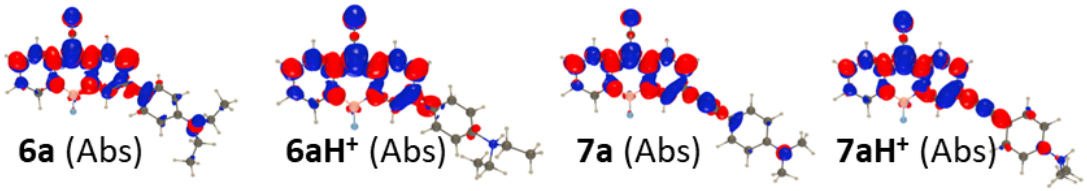

*Figure 12. Electron Density Difference (EDD) representation for both absorption of **6a** and **7a**, under neutral and protonated form. See caption of Figure 10 for more details.*

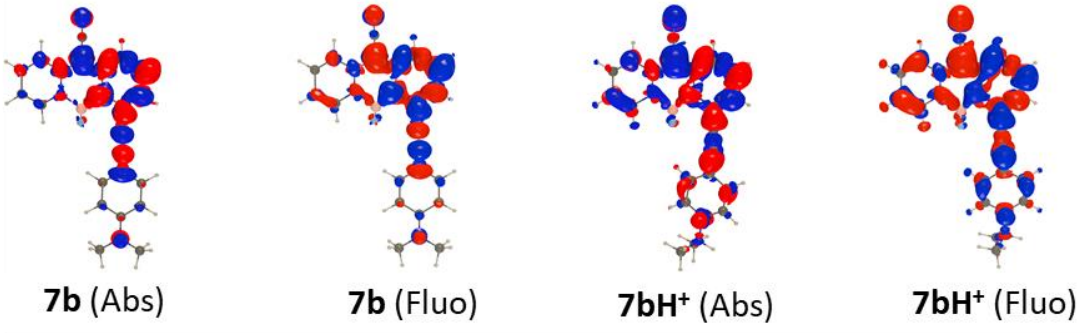

*Figure 13. Electron Density Difference (EDD) representation for both absorption and emission of **7b**. See caption of Figure 10 for more details.*

We have also estimated the singlet-triplet gaps and spin-orbit coupling (SOC) couplings for **2a** and **2b**, as well as **3a** and **3b**, the latter being used for comparison purposes. These calculations were performed on the relaxed S_1 geometry. In **2a**, the S_1-T_1 gap is -0.31 eV and the second triplet is more than 0.25 eV above the lowest singlet state. The SOC coupling was found to be moderate between the two lowest excited states of each spin symmetry, i.e., 0.36 cm^{-1}. A different picture is obtained in **2b**, with a S_1-T_1 gap of -0.24 eV and a strong SOC of 2.36 cm^{-1}, which is more favorable for ISC. In **3a** (**3b**), the S_1-T_1 gap is -0.29 eV (-0.21 eV), i.e., rather similar to the two previous compounds, but the SOC couplings are totally trifling: 0.01 cm^{-1} (0.07 cm^{-1}). These values are clearly in agreement with a very effective ISC in **2b**, that presents a very low fluorescence yield (0.01), an efficient one in **2a**, that presents a larger emission yield (0.03), and likely no significant ISC in the other compounds, a trend consistent with the presence of bromine atoms only in **2a** and **2b**.

Conclusions

In the present work we reported the synthesis of two series (**a** and **b**) of novel *meso*-CN BF_2-DIPYR complexes. Pd-catalyzed Suzuki-Miyaura cross coupling reaction on both 2- and 1-bromo *meso*-CN BF_2-DIPYR with various aryl boronic acids yielded efficiently mono-substituted derivatives bearing both electron-donating and electron-withdrawing groups. Similarly, the distance between the BF_2-DIPYR core and the aryl substituent could be controlled through the introduction of an aniline-substituted triple bond *via* a Pd-catalyzed Sonogashira cross coupling on either the halogenated boron complex or on the ligand before complexation. All derivatives were studied in detail, and, for each series, single crystals were obtained allowing the analysis of the molecular structure by X-ray diffraction. TD-DFT and CC2 calculations were also performed, and they showed very nice agreement with the experimental measurements. We demonstrated that in solution and according to the position on the aromatic core, the electronic nature of the substituents and the polarity of the environment, these

novel *meso*-CN BF_2-DIPYR complexes exhibited excellent fluorescence emission properties with colors from blue to orange upon blue light absorption. Remarkably, 1-aryl *meso*-CN BF_2-DIPYR complexes also showed large Stokes shifts values (>80 nm or >3000 cm^{-1}), [49] which open new opportunities for their biological application as imaging agents. Following the observation of their promising features as solid emitters, studies to optimize these structures to enhance the emissive properties in solid state are currently underway in our group.

Experimental section

Compounds **1a,b**[46] and **2a**[36] were prepared following literature procedures.

4-bromo-4a,5a-diaza-5,5-difluoro-5-bora-anthracene-10-carbonitrile (2b): NEt_3 (2.8 mL, 20.4 mmol) and $BF_3{\cdot}OEt_2$ (3.9 mL, 32.8 mmol) to a solution of *o*-Br-bis(2-pyridyl)acetonitrile (0.20 g, 0.73 mmol) in CH_2Cl_2 (70 mL) at room temperature and the mixture was subsequently refluxed in an oil bath for 72 h. After cooling down the reaction mixture, the solvent was partially removed under reduced pressure and the residue was first washed with water (x 3) and then purified *via* chromatography on SiO_2 (CH_2Cl_2) to give the product in 84% (220 mg, 0.68 mmol) as a yellow solid. ^{1}H NMR (500 MHz, $CDCl_3$): δ (ppm) 8.21 (br s, 1H), 7.76 (ddd, ^4J = 8.6, 7.0, 1.5 Hz, 1H), 7.56 (t, ^3J = 7.9 Hz, 2H), 7.42 (dd, ^4J = 8.8, 7.3 Hz, 1H), 7.14 (d, ^3J = 7.3 Hz, 1H), 6.99 (t, ^3J = 6.8 Hz, 1H). ^{13}C{H} NMR (125 MHz, $CDCl_3$): δ (ppm) 153.4 (C_q, 1C), 149.4 (C_q, 1C), 140.0 (CH, 1C), 138.9 (CH, 2C), 130.9 (C_q, 1C), 122.1 (CH, 1C), 119.9 (CH, 1C), 118.9 (C_q, 1C), 115.9 (CH, 1C). ^{19}F NMR (470 MHz, $CDCl_3$): δ (ppm) -122.1 (q, J = 31.5 Hz). ^{11}B NMR (160.5 MHz, $CDCl_3$): δ (ppm) 1.58 (t, J = 31.5 Hz). HRMS (ESI-TOF) *m/z*: [M+H] calcd for $C_{12}H_8BBrF_2N_3$: 321.995723; found 321.993302.

General procedure for the Suzuki-Miyaura cross coupling (GP1)

$Pd(PPh_3)_2Cl_2$ (0.02 mmol, 0.1 eq.) and K_2CO_3 (2 M in water, 8.0 eq.) are added to a degassed solution of 2a or 2b (0.16 mmol, 1.0 eq.) and boronic acids a-e (0.23 mmol, 1.5 eq.) in 1,4-dioxane/EtOH (2/3, 0.04 M) or in toluene (0.04 M) at room temperature and under a positive pressure of argon. The reaction mixture is warmed up to 80 °C in an oil bath and stirred for 18 h. The solvent is then removed under reduced pressure and the residue purified by column chromatography on SiO_2.

General procedure for the Sonogashira cross coupling (GP2)

$Pd(dppf)Cl_2$ (0.02 mmol, 0.1 eq.), CuI (0.02 mmol, 0.1 eq.) and NEt_3 (0.02 M) are added to a degassed solution of 2b or 8 (0.16 mmol, 1.0 eq.) and alkyne (0.19 mmol, 1.5 eq.) in toluene (0.04 M) at room temperature and under a positive pressure of argon. The reaction mixture is warmed up to 95 °C in an oil bath and stirred for 1 h. The solvent is then removed under reduced pressure and the residue purified by column chromatography on SiO_2.

3-(4'-methoxyphenyl)-4-bromo-4a,5a-diaza-5,5-difluoro-5-bora-anthracene-10-carbonitrile (3a): Compound 3a was obtained according to GP1 after purification on SiO_2 (petrol ether or PET/EtOAc, 1/1) in 70% yield (70 mg, 0.11 mmol) as a dark yellow solid. ^{1}H NMR (500 MHz, $CDCl_3$): δ (ppm) 8.34 (br s, 1H), 8.18 (br s, 1H), 7.94 (dd, ^4J = 9.1, 2.0 Hz, 1H), 7.70 (ddd, ^4J = 8.6, 6.9, 1.4 Hz, 1H), 7.63 (d, ^3J = 9.1 Hz, 1H), 7.57 (d, ^3J = 8.8 Hz, 1H), 7.49 (d, ^3J = 8.8 Hz, 2H), 7.01 (d, ^3J = 8.8 Hz, 2H), 6.92 (t, ^3J = 6.6 Hz, 1H), 3.87 (s, 3H). ^{13}C{H} NMR (125 MHz, $CDCl_3$): δ (ppm) 160.2 (C_q, 2H), 150.4 (C_q, 1C), 148.7 (C_q, 1C), 139.4 (CH, 1C), 139.2 (CH, 1C), 138.0 (CH, 1C), 135.0 (CH, 1C), 129.1 (C_q, 1C), 128.0 (C_q, 2C), 127.6 (CH, 2C), 120.4 (CH, 1C), 120.3 (CH, 1C), 119.2 (C_q, 1C), 115.1 (CH, 1C), 115.0 (CH, 2C), 55.6 (CH_3, 1C). ^{19}F NMR (470 MHz, $CDCl_3$): δ (ppm) -138.5 (q, J = 29.9 Hz). ^{11}B NMR (160.5 MHz, $CDCl_3$): δ (ppm) 1.43 (t, J = 29.8 Hz). HRMS (ESI-TOF) *m/z*: [M+H] calcd for $C_{19}H_{15}BF_2N_3O$: 350.1271; found 350.1259.

3-(4'-fluorophenyl)-4-bromo-4a,5a-diaza-5,5-difluoro-5-bora-anthracene-10-carbonitrile (4a): Compound 4a was obtained according to GP1 after purification on SiO_2 (PET/EtOAc, 1/1) in 88% yield (46 mg, 0.14 mmol) as a yellow solid. ^{1}H NMR (500 MHz, $CDCl_3$): δ (ppm) 8.32 (br s, 1H), 8.19 (br s, 1H), 7.91 (dd, ^4J = 9.1, 2.1 Hz, 1H), 7.73 (ddd, ^4J = 8.6, 7.0, 1.4 Hz, 1H), 7.63 (d, ^3J = 9.1 Hz, 1H), 7.58 (d, ^3J = 8.8 Hz, 1H), 7.50-7.54 (m, 2H), 7.15-7.21 (m, 2H), 6.96 (t, ^3J = 6.7 Hz, 1H). ^{13}C{H} NMR (125 MHz, $CDCl_3$): δ (ppm) 164.4 (C_q, 2C), 161.9 (C_q, 1C), 150.5 (C_q, 1C), 149.1 (C_q, 1C), 139.3 (CH, 1C), 139.5 (CH, 1C), 138.3 (CH, 1C), 138.1 (CH, 1C), 135.4 (CH, 1C), 131.8 (d, J = 3.5 Hz, C_q, 1C), 128.2 (d, J = 8.3 Hz, CH, 2C), 120.6 (CH, 1C), 120.3 (CH, 1C), 119.0 (C_q, 1C), 116.6 (d, J = 21.8, CH, 2C), 115.4 (CH, 1C). ^{19}F NMR (470 MHz, $CDCl_3$): δ (ppm) -138.2 (q, J = 29.8 Hz), -113.0 (s). ^{11}B NMR (160.5 MHz, $CDCl_3$): δ (ppm) 1.44 (t, J = 29.8 Hz). HRMS (ESI-TOF) *m/z*: [M+H] calcd for $C_{18}H_{12}BF_3N_3$: 338.1071; found 338.1053.

3-(4'-cyanophenyl)-4-bromo-4a,5a-diaza-5,5-difluoro-5-bora-anthracene-10-carbonitrile (5a): Compound 5a was obtained according to GP1 after purification on SiO_2 (PET/EtOAc, 7/3) in 86% yield (46 mg, 0.14 mmol) as a yellow solid. ^{1}H NMR (500 MHz, $CDCl_3$): δ (ppm) 8.39 (br s, 1H), 8.25 (br s, 1H), 7.93 (dd, ^4J = 9.2, 2.1 Hz, 1H), 7.77-7.81 (m, 3H), 7.62-7.69 (m, 4H), 7.03 (t, ^3J = 6.5 Hz, 1H). ^{13}C{H} NMR (125 MHz, $CDCl_3$): δ (ppm) 150.4 (C_q, 1C), 149.8 (C_q, 1C), 140.0 (C_q, 1C), 140.0 (CH, 1C), 138.3 (CH, 1C), 137.6 (CH, 1C), 136.3 (CH, 1C), 133.3 (CH, 2C), 126.9 (CH, 2C), 126.6 (C_q, 1C), 120.9 (CH, 1C), 120.5 (CH, 1C), 118.6 (C_q, 1C), 118.5 (C_q, 2C), 116.1 (CH, 1C), 112.3 (C_q, 1C). ^{19}F NMR (470 MHz, $CDCl_3$): δ (ppm) -138.0 (q, J = 29.7 Hz). ^{11}B NMR (160.5 MHz, $CDCl_3$): δ (ppm) 1.42 (t, J = 29.7 Hz). HRMS (ESI-TOF) *m/z*: [M+H] calcd for $C_{19}H_{12}BF_2N_4$: 345.1118; found 345.1115. M.p: 269.6-270.3 °C.

3-(4'-((diethylamino)phenyl))-4-bromo-4a,5a-diaza-5,5-difluoro-5-bora-anthracene-10-carbonitrile (6a): Compound 6a was obtained according to GP1 after purification on SiO_2 (toluene) in 66% yield (40 mg, 0.10 mmol) as a dark yellow solid. ^{1}H NMR (500 MHz, $CDCl_3$): δ (ppm) 8.34 (br s, 1H), 8.15 (br s, 1H), 7.95 (dd, ^4J = 9.1, 2.1 Hz, 1H), 7.66 (ddd, ^4J = 8.6, 6.9, 1.5 Hz, 1H), 7.60 (d, ^3J = 9.1 Hz, 1H), 7.54 (d, ^3J = 8.9 Hz, 2H), 7.42 (d, ^3J = 8.9 Hz, 2H), 6.87 (t, ^3J = 6.6 Hz, 1H), 6.75 (d, ^3J = 8.9 Hz, 2H), 3.41 (q, ^3J = 7.1 Hz, 4H), 1.20 (t, ^3J = 7.1 Hz, 6H). ^{13}C{H} NMR (125 MHz, $CDCl_3$): δ (ppm) 150.6 (C_q, 1C), 148.1 (C_q, 1C), 147.8 (C_q, 1C), 138.9 (CH, 1C), 138.0 (CH, 1C), 134.0 (CH, 1C), 129.9 (C_q, 1C), 127.3 (CH, 2C), 121.8 (C_q, 1C), 120.3 (CH, 1C), 119.4 (C_q, 1C), 114.6 (CH, 1C), 112.2 (CH, 2C), 44.6 (CH_2, 2C), 12.7 (CH_3, 2C). ^{19}F NMR (470 MHz, $CDCl_3$): δ (ppm) -138.8 (q, J = 29.9 Hz). ^{11}B NMR (160.5 MHz, $CDCl_3$): δ (ppm) 1.44 (t, J = 29.9 Hz). HRMS (ESI-TOF) *m/z*: [M+H] calcd for $C_{22}H_{22}BF_2N_4$: 391.1900; found 391.1900.

3-(4'-((dimethylamino)phenyl)ethynyl)-4-bromo-4a,5a-diaza-5,5-difluoro-5-bora-anthracene-10-carbonitrile 7a: Compound 7a was obtained according to GP2 after purification on SiO_2 (PET/EtOAc, 7/3) in 84% yield (50 mg, 0.13 mmol) as a dark yellow solid. ^{1}H NMR (500 MHz, $CDCl_3$): δ (ppm) 8.30 (br s, 1H), 8.19 (br s, 1H), 7.70-7.75 (m, 2H), 7.58 (d, ^3J = 8.9 Hz, 1H), 7.49 (d, ^3J = 9.0 Hz, 2H), 7.39 (d, ^3J = 8.9 Hz, 2H), 6.96 (t, ^3J = 6.7 Hz, 1H), 6.66 (d, ^3J = 9.0 Hz, 2H), 3.01 (s, 6H). ^{13}C{H} NMR (125 MHz, $CDCl_3$): δ (ppm) 150.6 (C_q, 2C), 150.3 (C_q, 1C), 148.3 (C_q, 1C), 140.9 (CH, 1C), 140.3 (CH, 1C), 139.5 (CH, 1C), 138.3 (CH, 1C), 133.0 (CH, 2C), 120.4 (CH, 1C), 119.8 (CH, 1C), 118.8 (C_q, 1C), 115.5 (CH, 1C), 113.1 (C_q, 1C), 111.9 (CH, 2C), 108.7 (C_q, 1C), 94.7 (C_q, 1C), 82.5 (C_q, 1C), 40.3 (CH_3, 2C). ^{19}F NMR (470 MHz, $CDCl_3$): δ (ppm) -138.5 (q, J = 29.6 Hz). ^{11}B NMR (160.5 MHz, $CDCl_3$): δ (ppm) 1.25 (t, J = 29.6 Hz). HRMS (ESI-TOF) *m/z*: [M+H] calcd for $C_{22}H_{18}BF_2N_4$: 387.1587; found 387.1590.

4-(4'-methoxyphenyl)-4-bromo-4a,5a-diaza-5,5-difluoro-5-bora-anthracene-10-carbonitrile (3b): Compound 3b was obtained according to GP1 after purification on SiO_2 (toluene) in 39% yield (21 mg, 0.06 mmol) as a dark yellow solid. ^{1}H NMR (500 MHz, $CDCl_3$): δ (ppm) 7.98 (br s, 1H), 7.62-7.68 (m, 3H), 7.52 (d, ^3J = 8.8 Hz, 1H), 7.39 (d, ^3J = 8.7 Hz, 2H), 6.95-6.99 (m, 2H), 6.81 (t, ^3J = 6.6 Hz, 1H), 6.69 (dd, ^4J = 5.9, 2.4 Hz, 1H), 3.87 (s, 3H). ^{13}C{H} NMR (125 MHz, $CDCl_3$): δ (ppm) 160.1 (C_q, 2C), 153.4 (C_q, 1C),

151.6 (C_q, 1C), 150.1 (C_q, 1C), 139.3 (CH, 1C), 138.4 (CH, 1C), 138.1 (t, *J* = 2.6 Hz, CH, 1C), 130.4 (t, *J* = 3.1 Hz, CH, 2C), 129.8 (C_q, 1C), 119.7 (CH, 1C), 119.6 (CH, 1C), 119.5 (CH, 1C), 114.9 (CH, 1C), 113.0 (CH, 2C), 55.3 (CH_3, 1C). ^{19}F NMR (470 MHz, $CDCl_3$): δ (ppm) -123.8 (q, *J* = 32.0 Hz). ^{11}B NMR (160.5 MHz, $CDCl_3$): δ (ppm) 1.57 (t, *J* = 32.0 Hz). HRMS (ESI-TOF) m/z: [M+H] calcd for $C_{19}H_{15}BF_2N_3O$: 350.1271; found 350.1241.

4-(4'-fluorophenyl)-4-bromo-4a,5a-diaza-5,5-difluoro-5-bora-anthracene-10-carbonitrile (4b): Compound 4b was obtained according to GP1 after purification on SiO_2 (toluene) in 53% yield (28 mg, 0.08 mmol) as a yellow solid. ^{1}H NMR (500 MHz, $CDCl_3$): δ (ppm) 7.97 (br s, 1H), 7.64-7.70 (m, 3H), 7.53 (d, ^3J = 8.8 Hz, 1H), 7.43 (dd, ^4J = 8.5, 5.4 Hz, 2H), 7.10-7.16 (m, 2H), 6.84 (t, ^3J = 6.6 Hz, 1H), 6.68 (dd, ^4J = 4.9, 3.4 Hz, 1H). ^{13}C{H} NMR (125 MHz, $CDCl_3$): δ (ppm) 164.3 (C_q, 1C), 161.8 (C_q, 1C), 152.0 (d, *J* = 56.1 Hz, C_q, 1C), 150.0 (C_q, 1C), 139.5 (CH, 1C), 139.3 (CH, 1C), 138.3 (CH, 1C), 138.1 (t, *J* = 2.6 Hz, CH, 1C), 133.3 (C_q, 1C), 131.0 (dt, *J* = 8.2, 3.3 Hz, CH, 2 C), 120.2 (CH, 1C), 119.7 (CH, 1C), 119.5 (C_q, 1C), 119.1 (CH, 1C), 115.2 (dd, *J* = 3.0, 1.7 Hz, CH, 1C), 114.7 (d, *J* = 21.8 Hz, CH, 2C). ^{19}F NMR (470 MHz, $CDCl_3$): δ (ppm) -123.2 (q, *J* = 32.1 Hz), -112.1 (s). ^{11}B NMR (160.5 MHz, $CDCl_3$): δ (ppm) 1.53 (t, *J* = 32.1 Hz). HRMS (ESI-TOF) m/z: [M+H] calcd for $C_{18}H_{12}BF_3N_3$: 338.1071; found 338.1068.

4-(4'-cyanophenyl)-4-bromo-4a,5a-diaza-5,5-difluoro-5-bora-anthracene-10-carbonitrile (5b): Compound 5b was obtained according to GP1 after purification on SiO_2 (toluene) in 62% yield (33 mg, 0.10 mmol) as a yellow solid. ^{1}H NMR (500 MHz, $CDCl_3$): δ (ppm) 7.96 (br s, 1H), 7.66-7.75 (m, 5H), 7.56-7.58 (m, 3H), 6.89 (t, ^3J = 6.7 Hz, 1H), 6.64 (dd, ^4J = 5.6, 2.6 Hz, 1H). ^{13}C{H} NMR (125 MHz, $CDCl_3$): δ (ppm) 151.8 (C_q, 1C), 150.8 (C_q, 1C), 149.9 (C_q, 1C), 141.7 (C_q, 1C), 139.8 (CH, 1C), 138.2 (t, *J* = 2.1 Hz, CH, 1C), 138.1 (CH, 1C), 131.5 (CH, 2C), 130.0 (t, *J* = 3.2 Hz, CH, 2C), 120.9 (CH, 1C), 119.9 (CH, 1C), 119.2 (C_q, 1C), 118.5 (C_q, 2C), 118.4 (CH, 1C), 115.7 (CH, 1C), 113.1 (C_q, 1C). ^{19}F NMR (470 MHz, $CDCl_3$): δ (ppm) -122.9 (q, *J* = 32.3 Hz). ^{11}B NMR (160.5 MHz, $CDCl_3$): δ (ppm) 1.52 (t, *J* = 32.3 Hz). HRMS (ESI-TOF) m/z: [M+H] calcd for $C_{19}H_{12}BF_2N_4$: 345.1118; found 345.1115. M.p: 226.0-226.5 °C.

4-(4'-((diethylamino)phenyl))-4-bromo-4a,5a-diaza-5,5-difluoro-5-bora-anthracene-10-carbonitrile (6b): Compound 6b was obtained according to GP1 after purification on SiO_2 (toluene) in 55% yield (33 mg, 0.08 mmol) as an orange solid. ^{1}H NMR (500 MHz, $CDCl_3$): δ (ppm) 8.02 (br s, 1H), 7.61-7.65 (m, 3H), 7.50 (d, ^3J = 8.8 Hz, 1H), 7.32 (d, ^3J = 8.7 Hz, 2H), 6.78 (t, ^3J = 6.6 Hz, 1H), 6.73 (d, ^3J = 6.6 Hz, 1H), 6.70 (d, ^3J = 8.9 Hz, 2H), 3.41 (q, ^3J = 7.1 Hz, 4H), 1.21 (t, ^3J = 7.1 Hz, 6H). ^{13}C{H} NMR (125 MHz, $CDCl_3$): δ (ppm) 154.8 (C_q, 1C), 151.7 (C_q, 1C), 150.2 (C_q, 1C), 148.2 (C_q, 2C), 139.1 (CH, 1C), 138.4 (CH, 1C), 138.1 (t, *J* = 1.9 Hz, CH, 1C), 130.2 (t, *J* = 3.5 Hz, CH, 2C), 124.1 (C_q, 1C), 120.0 (C_q, 1C), 119.9 (CH, 1C), 119.6 (CH, 1C), 119.0 (CH, 1C), 114.6 (CH, 1C), 110.1 (CH, 2C), 44.4 (CH_2, 2C), 12.8 (CH_3, 2C),. ^{19}F NMR (470 MHz, $CDCl_3$): δ (ppm) -124.9 (q, *J* = 31.8 Hz). ^{11}B NMR (160.5 MHz, $CDCl_3$): δ (ppm) 1.57 (t, *J* = 31.8 Hz). HRMS (ESI-TOF) m/z: [M+H] calcd for $C_{22}H_{22}BF_2N_4$: 391.1900; found 391.1888.

2-(6-((4-(dimethylamino)phenyl)ethynyl)pyridin-2(1*H*)-ylidene)-2-(pyridin-2-yl)acetonitrile (8): Compound 8 was obtained according to GP2 after purification on SiO_2 (CH_2Cl_2/MeOH 99.5/0.5) in 51% yield (62 mg, 0.18 mmol) as red solid. ^{1}H NMR (500 MHz, $CDCl_3$): δ (ppm) 16.3 (s, 1H), 7.89 (m, 1H), 7.49 – 7.41 (m, 4H), 7.39 (dq, ^4J = 8.9, 1.1 Hz, 1H), 7.31 (dd, ^4J = 8.7, 1.1 Hz, 1H), 6.84 (d, ^3J = 7.3 Hz, 1H), 6.70 – 6.66 (m, 2H), 6.59 (t, ^3J = 6.4 Hz, 1H), 3.03 (s, 6H). ^{13}C{H} NMR (125 MHz, $CDCl_3$): δ (ppm) 156.1, 155.1, 150.9, 138.2, 136.8, 136.4, 135.7, 133.4, 122.5, 120.4, 118.6, 117.3, 112.4, 111.9, 108.2, 93.4, 85.1, 68.4, 40.3. HRMS (ESI-TOF) m/z: [M+H] calcd for $C_{22}H_{19}N_4$: 339.1604; found 339.1602.

4-(4'-((dimethylamino)phenyl)ethynyl)-4-bromo-4a,5a-diaza-5,5-difluoro-5-bora-anthracene-10-carbonitrile (7b): NEt_3 (0.38 mL, 2.52 mmol) and $BF_3{\cdot}OEt_2$ (0.33 mL, 2.70 mmol) to a solution of

compound **8** (0.062 g, 0.18 mmol) in CH_2Cl_2 (20 mL) at room temperature and the mixture was subsequently refluxed in an oil bath for 3 h. After cooling down the reaction mixture, the solvent was partially removed under reduced pressure and the residue was first washed with water (x 3) and then purified *via* chromatography on SiO_2 (PET/EtOAc, 1/1) to obtain complex 7b in 14% yield (10 mg, 0.03 mmol) as orange solid. ^{1}H NMR (500 MHz, $CDCl_3$): δ (ppm) 8.25 (br s, 1H), 7.69 (t, ^3J = 8.1 Hz, 1H), 7.60 – 7.43 (m, 5H), 7.08 (d, ^3J = 7.3 Hz, 1H), 6.90 (t, ^3J = 6.7 Hz, 1H), 6.67 (d, ^3J = 8.5 Hz, 2H), 3.03 (s, 6H). ^{11}B NMR (160.5 MHz, $CDCl_3$): δ (ppm) 1.70 (t, J = 31.0 Hz). HRMS (ESI-TOF) m/z: [M+H] calcd for $C_{22}H_{18}BF_2N_4$: 387.1587; found 387.1588. Because of the poor solubility of **7b** in organic solvents and so in CDCl3, a ^{13}C{H} NMR could not be obtained.

Data Availability Statement

The data underlying this study are available in the published article and its Supporting Information.

Supporting Information

The Supporting Information file is available free of charge. ^{1}H and ^{13}C NMR spectra, HRMS spectra, spectroscopic data, X-ray analyses, and details of the computational procedures and Cartesian coordinates are included (PDF).

Acknowledgements

C. F. thanks the Interdisciplinary Institute HiFunMat for support of the SMARTY starting grant. This work of the Interdisciplinary Institute HiFunMat, as part of the ITI 2021–2028 program of the University of Strasbourg, CNRS and Inserm, was supported by IdEx Unistra (ANR-10-IDEX-0002) and SFRI (STRAT'US project, ANR-20-SFRI-0012) under the framework of the French Investments for the Future Program. T.V.P., D.J. and G.U. are indebted to the ANR for support in the framework of the BiBiFlu grant (ANR-21-CE43-0019). Furthermore, the Nantes' team thanks the CCIPL/GliciD computational center for generous allocation of computational resources.

References

(1) Wu, J.; Shi, Z.; Zhu, L.; Li, J.; Han, X.; Xu, M.; Hao, S.; Fan, Y.; Shao, T.; Bai, H.; Peng, P.; Hu, W.; Liu, X.; Yao, C.; Li, L.; Huang, W. The Design and Bioimaging Applications of NIR Fluorescent Organic Dyes with High Brightness. *Adv. Optical Mater.* **2022**, *10*, 2102514.

(2) Hao, Q.; Yu, S.; Li, S.; Chen, J.; Zeng, Y.; Yu, T.; Yang, G.; Li, Y. Locked Planarity: A Strategy for Tailoring Ladder-Type π-Conjugated Anilido–Pyridine Boron Difluorides. *J. Org. Chem.* **2014**, *79*, 459-464.

(3) Chen, X.; Tan, D.; Yang, D.-T. Multiple-boron–nitrogen (multi-BN) doped π-conjugated systems for optoelectronics. *J. Mater. Chem. C* **2022**, *10*, 13499-13532.

(4) Dewar, M. J. S.; Dietz, R. 546. New heteroaromatic compounds. Part III. 2,1-Borazaro-naphthalene (1,2-dihydro-1-aza-2-boranaphthalene). *J. Chem. Soc.* **1959**, 2728-2730.

(5) Paetzold, P.; Stanescu, C.; Stubenrauch, J. R.; BienmLler, M.; Englert, U. 1-Azonia-2-boratanaphthalenes. *Z. Anorg. Allg. Chem.* **2004**, *630*, 2632-2640.

(6) Mercier, L. G.; Piers, W. E.; Parvez, M. Benzo- and Naphthoborepins: Blue-Emitting Boron Analogues of Higher Acenes. *Angew. Chem. Int. Ed.* **2009**, *48*, 6108-6111.

(7) Bosdet, M. J. D.; Piers, W. E.; Sorensen, T. S.; Parvez, M. 10a-Aza-10b-borapyrenes: Heterocyclic Analogues of Pyrene with Internalized BN Moieties. *Angew. Chem.* **2007**, *119*, 5028-5031.

(8) Von Grotthuss, E.; John, A.; Kaese, T.; Wagner, M. Doping Polycyclic Aromatics with Boron for Superior Performance in Materials Science and Catalysis. *Asian J. Org. Chem.* **2018**, *7*, 37-53.

(9) Frath, D.; Massue, J.; Ulrich, G.; Ziessel, R. Luminescent Materials: Locking π-Conjugated and Heterocyclic Ligands with Boron(III). *Angew. Chem. Int. Ed.* **2014**, *53*, 2290-2310.

(10) Curiel, D.; Más-Montoya, M.; Usea, L.; Espinosa, A.; Orenes, R. A.; Molina, P. Indolocarbazole-Based Ligands for Ladder-Type Four-Coordinate Boron Complexes. *Org. Lett.* **2012**, *14*, 3360-3363.
(11) Más-Montoya, M.; Montenegro, M. F.; Espinosa Ferao, A.; Tárraga, A.; Rodríguez-López, J. N.; Curiel, D. Rigid π-Extended Boron Difluoride Complex with Mega-Stokes Shift for Bioimaging. *Org. Lett.* **2020**, *22*, 3356-3360.
(12) Ulrich, G.; Ziessel, R.; Harriman, A. The Chemistry of Fluorescent Bodipy Dyes: Versatility Unsurpassed. *Angew. Chem. Int. Ed.* **2008**, *47*, 1184-1201.
(13) Mula, S.; Leclerc, N.; Lévêque, P.; Retailleau, P.; Ulrich, G. Synthesis of Indolo[3,2-b]carbazole-Based Boron Complexes with Tunable Photophysical and Electrochemical Properties. *J. Org. Chem.* **2018**, *83*, 14406-14418.
(14) Tanaka, K.; Gon, M.; Ito, S.; Ochi, J.; Chujo, Y. Recent progresses in the mechanistic studies of aggregation-induced emission-active boron complexes and clusters. *Coord. Chem. Rev.* **2022**, *472*, 214779.
(15) Yu, C.; Hao, E.; Sun, Y.; Jiao, L. Recent Advances in Highly Fluorescent Hydrazine-Inserted Pyrrole-Based Diboron-Anchoring Fluorophores: Synthesis and Properties. *Synlett* **2023**, *34*, A-R.
(16) Bismillah, A. N.; Aprahamian, I. Boron difluoride hydrazone (BODIHY) complexes: A new class of fluorescent molecular rotors. *J. Phys. Org. Chem.* **2023**, *36*, e4485.
(17) Lu, H.; Mack, J.; Nyokong, T.; Kobayashi, N.; Shen, Z. Optically active BODIPYs. *Coord. Chem. Rev.* **2016**, *318*, 1-15.
(18) Poddar, M.; Misra, R. Recent advances of BODIPY based derivatives for optoelectronic applications. *Coord. Chem. Rev.* **2020**, *421*, 213462.
(19) Zhang, W.; Ahmed, A.; Cong, H.; Wang, S.; Shen, Y.; Yu, B. Application of multifunctional BODIPY in photodynamic therapy. *Dyes Pigm.* **2021**, *185*, 108937.
(20) Bumagina, N. A.; Antina, E. V.; Ksenofontov, A. A.; Antina, L. A.; Kalyagin, A. A.; Berezin, M. B. Basic structural modifications for improving the practical properties of BODIPY. *Coord. Chem. Rev.* **2022**, *469*, 214684.
(21) Yuan, L.; Su, Y.; Cong, H.; Yu, B.; Shen, Y. Application of multifunctional small molecule fluorescent probe BODIPY in life science. *Dyes and Pigments* **2023**, *208*, 110851.
(22) Mao, Z.; Kim, J. H.; Lee, J.; Xiong, H.; Zhang, F.; Kim, J. S. Engineering of BODIPY-based theranostics for cancer therapy. *Coord. Chem. Rev.* **2023**, *476*, 214908.
(23) Cheng, H. B.; Cao, X.; Zhang, S.; Zhang, K.; Cheng, Y.; Wang, J.; Zhao, J.; Zhou, L.; Liang, X. J.; Yoon, J. BODIPY as a Multifunctional Theranostic Reagent in Biomedicine: Self-Assembly, Properties, and Applications. *Adv. Mater.* **2023**, *35*, 2207546.
(24) Wang, D.; Wang, X.; Zhou, S.; Gu, P.; Zhu, X.; Wang, C.; Zhang, Q. Evolution of BODIPY as triplet photosensitizers from homogeneous to heterogeneous: The strategies of functionalization to various forms and their recent applications. *Coord. Chem. Rev.* **2023**, *482*, 215074.
(25) Liu, Z.; Jiang, Z.; Yan, M.; Wang, X. Recent Progress of BODIPY Dyes With Aggregation-Induced Emission. *Front. Chem.* **2019**, *7*, 712.
(26) Shamova, L. I.; Zatsikha, Y. V.; Nemykin, V. N. Synthesis pathways for the preparation of the BODIPY analogues: aza-BODIPYs, BOPHYs and some other pyrrole-based acyclic chromophores. *Dalton Trans.* **2021**, *50*, 1569-1593.
(27) Alsimaree, A. A.; Alatawi, O. M.; Waddell, P. G.; Day, D. P.; Alsenani, N. I.; Knight, J. G. Pyrrolylquinoline-BF_2 and BPh_2 BODIPY-Type Analogues: Synthesis, Structural Analysis and Photophysical Properties. *Crystals* **2021**, *11*, 1103.
(28) Nakano, T.; Sumida, A.; Naka, K. 2-(Quinol-8-yl)pyrrole-Boron Difluoride Complexes, Simple and Tractable Structures Exhibiting Red Emission. *ChemistrySelect* **2021**, *6*, 1168-1173.
(29) Araneda, J. F.; Piers, W. E.; Heyne, B.; Parvez, M.; McDonald, R. High Stokes Shift Anilido-Pyridine Boron Difluoride Dyes. *Angew. Chem. Int. Ed.* **2011**, *50*, 12214-12217.
(30) Liu, S.-F.; Wu, Q.; Schmider, H. L.; Aziz, H.; Hu, N.-X.; Popović, Z.; Wang, S. Syntheses, Structures, and Electroluminescence of New Blue/Green Luminescent Chelate Compounds: $Zn(2\text{-py-in})_2(THF)$, $BPh_2(2\text{-py-in})$, $Be(2\text{-py-in})_2$, and $BPh_2(2\text{-py-aza})$ [2-py-in) 2-(2-pyridyl)indole; 2-py-aza) 2-(2-pyridyl)-7-azaindole]. *J. Am. Chem. Soc.* **2000**, *122*, 3671-3678.

(31) Liu, Q.; Mudadu, M. S.; Schmider, H.; Thummel, R.; Tao, Y.; Wang, S. Tuning the Luminescence and Electroluminescence of Diphenylboron Complexes of 5-Substituted 2-(2'-Pyridyl)indoles. *Organometallics* **2002**, *21*, 4743-4749.
(32) Liu, Q. D.; Mudadu, M. S.; Thummel, R.; Tao, Y.; Wang, S. From Blue to Red: Syntheses, Structures, Electronic and Electroluminescent Properties of Tunable Luminescent N,N Chelate Boron Complexes. *Adv. Funct. Mater.* **2005**, *15*, 143-154.
(33) Jin, J.-L.; Li, H.-B.; Geng, Y.; Wu, Y.; Duan, Y.-A.; Su, Z.-M. Theoretical Insight into the Origin of Large Stokes Shift and Photophysical Properties of Anilido-Pyridine Boron Difluoride Dyes. *ChemPhysChem* **2012**, *13*, 3714-3722.
(34) Douglass, J. E.; Barelski, P. M.; Blankenship, R. M. Diazaboracyclic cations. III. A homomorph of 9,10-dihydroanthracene. *J. Heterocycl. Chem.* **1973**, *10*, 255-257.
(35) Sathyamoorthi, G.; Soong, M.-L.; Ross, T. W.; Boyer, J. H. Fluorescent tricyclic beta-azavinamidine-BF_2 complexes. *Heteroatom Chem.* **1993**, *4*, 603-608.
(36) Kubota, Y.; Tsuzuki, T.; Funabiki, K.; Ebihara, M.; Matsui, M. Synthesis and Fluorescence Properties of a Pyridomethene−BF_2 Complex. *Org. Lett.* **2010**, *12*, 4010-4013.
(37) Lin, Y.-D.; Chow, T. J. A pyridomethene–BF_2 complex-based chemosensor for detection of hydrazine. *RSC Adv.* **2013**, *3*, 17924-17929.
(38) Lin, Y.-D.; Ke, B.-Y.; Chang, Y. J.; Chou, P.-T.; Liau, K.-L.; Liu, C.-Y.; Chow, T. J. Pyridomethene–BF_2 complex/phenothiazine hybrid sensitizer with high molar extinction coefficient for efficient, sensitized solar cells. *J. Mater. Chem. A* **2015**, *3*, 16831-16842.
(39) Golden, J. H.; Facendola, J. W.; Sylvinson M. R, D.; Baez, C. Q.; Djurovich, P. I.; Thompson, M. E. Boron Dipyridylmethene (DIPYR) Dyes: Shedding Light on Pyridine-Based Chromophores. *J. Org. Chem.* **2017**, *82*, 7215-7222.
(40) Golden, J. H.; Estergreen, L.; Porter, T.; Tadle, A. C.; Sylvinson M. R, D.; Facendola, J. W.; Kubiak, C. P.; Bradforth, S. E.; Thompson, M. E. Symmetry-Breaking Charge Transfer in Boron Dipyridylmethene (DIPYR) Dimers. *ACS Appl. Energy Mater.* **2018**, *1*, 1083-1095.
(41) Kondakova, M. E.; Deaton, J. C.; Pawlik, T. D.; Giesen, D. J.; Kondakov, D. Y.; Young, R. H.; Royster, T. L.; Comfort, D. L.; Shore, J. D. Highly efficient fluorescent-phosphorescent triplet-harvesting hybrid organic light-emitting diodes. *J. Appl. Phys.* **2010**, *107*, 014515.
(42) Bañuelos, J.; Arbeloa, F. L.; Martinez, V.; Liras, M.; Costela, A.; Moreno, I. G.; Arbeloa, I. L. Difluoro-boron-triaza-anthracene: a laser dye in the blue region. Theoretical simulation of alternative difluoro-boron-diaza-aromatic systems. *Phys. Chem. Chem. Phys.* **2011**, *13*, 3437-3445.
(43) Wang, D.; Liu, R.; Chen, C.; Wang, S.; Chang, J.; Wu, C.; Zhu, H.; Waclawik, E. R. Synthesis, photophysical and electrochemical properties of aza-boron-diquinomethene complexes. *Dyes Pigm.* **2013**, *99*, 240-249.
(44) Tadle, A. C.; El Roz, K. A.; Soh, C. H.; Sylvinson Muthiah Ravinson, D.; Djurovich, P. I.; Forrest, S. R.; Thompson, M. E. Tuning the Photophysical and Electrochemical Properties of Aza-Boron-Dipyridylmethenes for Fluorescent Blue OLEDs. *Adv. Funct. Mater.* **2021**, *31*, 2101175.
(45) Shi, Z.; Han, X.; Hu, W.; Bai, H.; Peng, B.; Ji, L.; Fan, Q.; Li, L.; Huang, W. Bioapplications of small molecule Aza-BODIPY: from rational structural design to *in vivo* investigations. *Chem. Soc. Rev.* **2020**, *49*, 7533-7567.
(46) Newkome, G. R.; Joo, Y. J.; Evans, D. W.; Pappalardo, S.; Fronczek, F. R. Nitrile-stabilized carbanions. Nucleophilic substitution reactions on bromopyridines. *J. Org. Chem.* **1988**, *53*, 786-790.
(47) Brock, C. P.; Dunitz, J. D. Temperature dependence of thermal motion in crystalline anthracene. *Acta Cryst.* **1990**, *46*, 795-806.
(48) Boeyens, J. C. A. The conformation of six-membered rings. *J. Crys. Mol. Struct.* **1978**, *8*, 317-320.
(49) Nakano, T.; Sumida, A.; Naka, K. Synthesis and Characterization of Boron Difluoride Complexes Bearing π-Expanded Pyridine Ligands as Organic Fluorochromes. *J. Org. Chem.* **2021**, *86*, 5690-5701.